Skeletal mechanism reduction through species-targeted sensitivity analysis.

A. Stagni[a], A. Frassoldati[a], A. Cuoci[a], T. Faravelli[a,*], E. Ranzi[a]

[a] *Department of Chemistry, Materials, and Chemical Engineering "G. Natta", Politecnico di Milano, 20133 Milano, Italy*

Abstract

The use of simplifying techniques to obtain skeletal kinetic mechanisms with the required accuracy is often a necessary step when computationally demanding simulations are concerned. In this work, a novel approach for an automatic mechanism reduction, aimed at retaining accuracy on specific target species, is proposed. Starting from the consolidated coupling between flux analysis and sensitivity analysis, a methodology based on curve matching and functional data analysis was developed, through which the importance of a species in the target accuracy is assessed via a proper metric. The error associated with the removal of uncertain species from the detailed mechanism is quantified in terms of distance and similarity indices before and after such a removal, within a Species-Targeted Sensitivity Analysis (STSA) framework. A species ranking is then generated, and the original mechanism is progressively reduced. The whole algorithm also implements several improvements to enhance a faster convergence, and adds a novel criterion to remove unimportant reactions, based on sensitivity analysis to kinetic parameters.

The capability of this algorithm was tested through two case studies in this work. A kinetic mechanism for a Toluene Reference Fuel (TRF) was first obtained, with the overall reactivity as reduction target. The numerical procedure allowed to obtain a compact skeletal mechanism (115 species and 856 reactions), able to retain good accuracy in ignition delay time and laminar flame speed predictions of both fuel mixture and pure compounds. More important, two skeletal mechanisms for methane combustion, including chemistry of nitrogen oxides (NO_x), were developed, with different degrees of reduction. The agreement between the original and the skeletal mechanisms in terms of NO formation was successfully assessed with satisfactory results. Attention was also dedicated to the choice of the type of reactor where undertaking reduction, which turned

out to play a major role in the overall process.

Keywords: Skeletal reduction, DRGEP, Sensitivity analysis, Pollutants, Curve matching

---

Nomenclature

Roman Symbols

P	Pressure
T	Temperature

Acronyms

DIC	Direct Interaction Coefficient
DRG	Directed Relation Graph
DRGASA	DRG-Aided Sensitivity Analysis
DRGEP	DRG with Error Propagation
DRGEPSA	DRG with Error Propagation and Sensitivity Analysis
MAD	Median Absolute Deviation
MPI	Message Passing Interface
NO_x	Nitrogen Oxides
ODE	Ordinary Differential Equation
OIC	Overall Interaction Coefficient
PAH	Polycyclic Aromatic Hydrocarbons
PRF	Primary Reference Fuel
PSR	Perfectly Stirred Reactor
STSA	Species-Targeted Sensitivity Analysis
TRF	Toluene Reference Fuel

Greek Symbols

$\hat{\varepsilon}_D$	Normalized L^2-distance index
$\hat{\varepsilon}_S$	Normalized similarity index
ρ	Restart factor in sensitivity analysis
τ	Reactor residence time

*Corresponding author. Phone: +39 02 2399 3282
Email address: tiziano.faravelli@polimi.it (T. Faravelli)

ε_D	L^2-distance index
ε_S	Similarity index
Φ	Equivalence ratio

Subscripts

i	Species index
j	Reaction index
k	Reactor index

1. Introduction

In order to ensure the necessary accuracy, high-fidelity models of combustion phenomena require a complete representation of the elementary reactions taking place among the different species involved in the modeled system. For this purpose, detailed kinetic mechanisms are developed for several classes of hydrocarbon fuels, which are validated in simple systems (e.g. ideal reactors) through comparison with experimental data. As one can imagine, their ultimate application lies in the numerical simulation of more complex flames in real systems. Here, the sole use of simplified mechanisms prevents a comprehensive study of such phenomena like the formation of pollutants (soot [1], NO_x [2], etc.), low-temperature combustion [3] and so on. Moreover, the implementation of detailed chemistry can significantly improve the reliability of turbulent simulations, which are based on a non-negligible number of hypotheses, and whose turbulent combustion models would greatly benefit from such an introduction [4].

Nevertheless, the complexity of detailed mechanisms may turn out as the limiting factor when they are applied to multidimensional models of combustion devices. Although the recent advancements in computation technology have allowed to use large kinetic schemes in the modeling of combustion chemistry, the detailed mechanisms of practical fuels, e.g. large hydrocarbons, are still limitedly applicable to 0D and 1D simulations. Moreover, for mechanisms also involving soot, aromatics or oxygenated species, the size of the model may easily explode, such that even the simulation of 1D systems become impractical. In this regard, the 2-methyl alkanes kinetic scheme developed by Sarathy et al. [5], made up of 7,175 species and 31,669 reactions, sets up an extreme example.

The impossibility to use most detailed kinetic models in complex simulations has paved the way, in the latest decades, to the research field of mechanism reduction. Several methodologies were developed to this purpose, and complete reviews of the state of the art were carried out by Lu and Law [6], and more recently by Turanyi and Tomlin [7]. As long as skeletal reduction approaches are concerned, they can be focused on the elimination of either reactions or species, which are considered as unimportant in the whole operating space of temperature, pressure, and equivalence ratio. Detecting the reactions which do not contribute to the formation of the investigated species is usually more direct, and several methods were developed to the purpose: among the others, Wang and Frenklach [8] proposed the detailed reduction method, while procedures based on sensitivity analysis were developed by Rabitz et al. [9] and Tomlin et al. [10]. Brown et al. [11] and Vajda et al. [12] applied the Principal Components Analysis (PCA) for reaction elimination. On the other hand, species-based elimination is more challenging because of the mutual coupling among species themselves, but it is much more effective from a computational point of view because it directly reduces the number of equations to be solved in the codes where the kinetic mechanism is applied. Therefore, significant research in this direction has been carried out in the latest decades. The most noticeable works in this field are based either on the analysis of the Jacobian matrix [13, 14] or, more recently, on flux analysis. In this regard, the method developed by Lu and Law [15] and known as Directed Relation Graph (DRG) made a significant breakthrough in mechanism reduction: by fixing a group of target species, this method estimates the importance of the remaining species in contributing to their formation. In the wake of DRG, other flux-based methods were developed, including DRG-Aided Sensitivity Analysis (DRGASA) [16], DRG with Error Propagation (DRGEP) [17], Path Flux Analysis (PFA) [18] and DRG with Error Propagation and Sensitivity Analysis (DRGEPSA) [19]. Each of them successfully improved the original formulation of the methodology, thus providing a reference framework for automatic mechanism reduction. On-the-fly techniques based on such approaches were also developed [20], and successfully coupled [21] to pre-existing tabulation-based methodologies [22].

Sensitivity-based reduction approaches like DRGASA and DRGEPSA were able to overcome the weaknesses of flux analysis. If on the one hand flux-based approaches

are particularly fast, on the other they are of limited use when a very high level of reduction is required. Therefore, at the price of a higher computing demand, sensitivity-based reductions are able to further push the degree of reduction with an acceptable preservation of accuracy. Nevertheless, the main limitation of such techniques lies in being targeted at fuel/air mixture reactivity (estimated through ignition delay time) as the only property to be preserved. Doing so, all the properties not directly related to it, like flame speed or species formation, are not under control and can then be compromised. A representative example in this direction is set up by the formation of pollutant species like Polycyclic Aromatic Hydrocarbons (PAH) and Nitrogen Oxides (NO_x), whose time scales are orders of magnitude higher than fuel ignition time.

The purpose of this work stems from the need to overcome such a limitation, and proposing a more comprehensive approach able to automatically keep the desired accuracy of skeletal mechanisms on the dynamics of defined target species, in addition to mixture reactivity. Starting from the described background, this paper presents a newer, generalized framework for the generation of skeletal mechanisms, which improves the established techniques through an extended sensitivity analysis, in order to achieve a final optimal reduction. The different steps of the proposed methodology are first described in Section 2, along with the respective strengths and weaknesses. A deeper insight into the theoretical aspects of Species-Targeted Sensitivity Analysis is then provided in Section 3. The whole approach is validated in Section 4, where two case studies are presented. Finally, conclusions are drawn in the last Section.

2. A divide-and-conquer, multi-step approach to skeletal reduction

As pointed out by Xin et al. [23], when a detailed mechanism is to be reduced, the original species may be divided into three subsets: critical, marginal, and nonessential. Once the range of operating conditions (i.e. temperature, pressure, and equivalence ratio) is identified, nonessential species are detected and eliminated quite straightforwardly, and a proper selection of marginal species is carried out, also according to the desired level of accuracy. As expectable, there is an opposite trend between the effectiveness of a given reduction technique and its computational demand. For this reason, the most performing strategies often consist of faster (and rougher) approaches on the initial mechanism, and

computationally heavier (but more accurate) techniques on already reduced models.

This procedure was followed in this work, too. As a first step, the detailed mechanism is reduced through DRGEP, thus cutting out the totally unnecessary species and retaining almost the total accuracy of the original model. Then, a dynamic sensitivity analysis on species is carried out on the uncertain species. As a last step, a sensitivity analysis on the kinetic parameters of the reactions allows the removal of the unimportant species. Each of these steps is described in this section, recalling the consolidated theoretical concepts and better focusing on the introduced novelties.

2.1. DRG with Error Propagation

A complete description of the original approach can be found in the work by Pepiot-Desjardins and Pitsch [17]. Therefore, only the main concepts are recalled, and framed into the overall procedure. DRGEP transforms the original kinetic mechanism into an equivalent graph, whose species constitute the vertices. These are connected through edges, whose strength depends on reactions linking them. In particular, in a given reaction state, the importance of species B in forming species A is estimated through the related Direct Interaction Coefficient (DIC):

$$r_{AB} = \frac{\left| \sum_{j=1}^{NR} \nu_{A,j} \omega_j \delta_j^B \right|}{max\left(P_A, C_A\right)} \tag{1}$$

where P_A and C_A are the Production and Consumption Rates of Species A, i.e.:

$$P_A = \sum_{i=1}^{NR} max(0, \nu_{A,i}\omega_i) \tag{2}$$

$$C_A = \sum_{i=1}^{NR} max(0, -\nu_{A,i}\omega_i) \tag{3}$$

δ_j^B is a boolean variable, indicating the presence of species B in the j-th reaction, $\nu_{A,j}$ is the stoichiometric coefficient of species A in the j-th reaction, and ω_j is the net reaction rate of the j-th reaction. Once one or more target species (e.g. fuel, oxygen, etc.) are set up, a path-dependent interaction coefficient is calculated through a damping procedure:

$$r_{AB,p} = \prod_{i=1}^{n_p - 1} r_{S_i S_{i+1}} \tag{4}$$

where S is the generic intermediate species, interposing in the p-th reaction path between the target species A and B. The overall interaction coefficient (OIC), representing the importance of species B for an accurate prediction of A, is then evaluated as:

$$R_{AB} = \max_{\text{all paths}} (r_{AB,p}) \tag{5}$$

Several algorithms can be adopted to find the shortest path, i.e. the path with the maximum product of DICs: Niemeyer and Sung [24] showed that Dijkstra's shortest paths algorithm [25] proved to be the most performing. If reaction state sampling is time-dependent (i.e., autoignition phenomena are analysed), these coefficients can then be corrected according to the scaling methodology proposed by Pepiot-Desjardins and Pitsch [17], which weighs them according to local reactivity. Finally, for each reactor the coefficient representing the importance of species B is then calculated by analyzing all target species and all reaction states, i.e.:

$$\widetilde{R}_B = \max_{X,t} R_{XB}(t) \tag{6}$$

The operating conditions where the mechanism is targeted at working are identified and set up in terms of (i) Temperature T, (ii) Pressure P and (iii) Equivalence Ratio Φ. Reaction state sampling can be carried out by using either transient or continuous, Perfectly Stirred Reactors (PSR) [26]; in this latter case a fourth dimension is added to the problem, i.e. residence time. The results of the overall process are, in principle, strongly dependent on this choice, as well as the range of applicability of the obtained mechanism (e.g. accuracy in flames prediction can be better predicted by PSRs, because of the more similar radical concentrations).

In this work, it is chosen to limit the state sampling to adiabatic batch reactors, and following what already done in literature [19], the generality of the skeletal mechanism was kept in DRGEP phase through conservative thresholds for species removal. Batch reactors can be chosen at constant pressure or volume according to the application which

they are intended to (e.g. atmospheric flame or internal combustion engine). The obtained reaction states were sampled and used to rank all the species according to $\tilde{R}_i$ (6). For each reactor, a threshold ε_{DRGEP} is set up (usually not higher than 10^{-3}) and fuel and oxidizer are considered as target species. The species with a value of $\tilde{R}_i$ higher than the threshold are then kept. Differently from the original approach, in this work a reduced mechanism for each sampled point of the $\mathrm{T}-\mathrm{P}-\Phi$ space is created according to the local ranking, in such a way to enhance the convergence of the overall procedure through a divide-and-conquer strategy. Deeper insight into it will be provided in the next Section.

2.2. Sensitivity analysis to ignition delay time

Flux-based approaches have the advantage of being very fast in determining a species ranking, since the required time for calculating production and consumption rates is a small fraction of the time required to carry out the integration of the Ordinary Differential Equation (ODE) system. On the other hand, when using flux analysis to obtain a significant reduction by increasing local thresholds, weaknesses come to light. Niemeyer et al. [19] showed that, for DRGEP, the correlation between species OIC and error induced by the removal of the species itself is far from linear: i.e., by increasing the threshold the risk of losing critical species increases, too, and these methods progressively lose their effectiveness. As a consequence, further reduction can be achieved using more time consuming approaches. Sensitivity analysis is then carried out by calculating the error on a defined target property following the removal of each of the analyzed species, and ranking them accordingly. Traditionally, the investigated property has been the ignition delay time in autoignition phenomena. This was introduced by Zheng et al. [16] through DRGASA approach, and then improved by Niemeyer et al. [19, 27] in the implementation of DRGEPSA. This approach was included in the present work, too, but with some modifications: starting from the local reduced mechanisms obtained for each sampled point through flux analysis, the respective subsets of species to be investigated are detected by fixing a threshold value of $\tilde{R}_i$ (6) (usually 0.1 can be used). The selection procedure of marginal species was refined through the addition of a parallel criterion,

based on the overall mass flux of the different species:

$$F_i = \frac{MW_i \cdot \int_0^{t_{ign}} (P_i + C_i)\, dt}{\max\left(MW_j \cdot \int_0^{t_{ign}} (P_j + C_j)\, dt\right)} \tag{7}$$

where MW_i is the molecular weight of the considered species, P_i and C_i were respectively defined in Eq. (2) and (3), and t_{ign} is the ignition delay time. A threshold value between 0.05 and 0.1 can be used for most applications. Since the i-th species is excluded from sensitivity analysis if it overcomes the threshold value in (6) and/or (7), this allows to reduce the size of the marginal species subsets, without significant effects on the size of the final mechanism.

Once detected, the marginal species are ranked according to the error induced by their removal: for the i-th species, such an error is evaluated as

$$\varepsilon_i = \frac{|\tau_{ign,i} - \tau_{DRGEP,i}|}{\tau_{DRGEP,i}} \tag{8}$$

where $\tau_{DRGEP,i}$ and $\tau_{ign,i}$ are the ignition delay times respectively before and after the removal. In this way, the species are ranked according to the induced error and can be then progressively removed from the mechanisms obtained in 2.1.

Adopting a local procedure allows to speed up significantly the iterative procedure, as the local mechanisms where such an analysis is carried out are smaller than the one obtained by directly merging the species subsets, as done for example in DRGASA. This allows to further refine the local convergence strategy: the frequent couplings among species cause a strong nonlinearity within the kinetic mechanism. Therefore, the ranking obtained cannot be considered as invariant throughout the removal procedure. A "restart factor" ρ is here introduced, such that species ranking is updated once σ_k/ρ species have been removed, with σ_k being the current size of the local marginal species subset for the k-th reactor. The choice of ρ depends on mechanism size and computational availability, but a convergence of final results was experienced for values of ρ higher than 5. A similar observation was also recently made by Niemeyer and Sung [27], who improved the original DRGEPSA through a *"greedy"* approach, based on global ranking recalculation at every species removal of coefficients.

This procedure is stopped when the error index reaches a defined threshold, and in this way the optimal species subset for each point of the $T - P - \Phi$ space is found. Then, the local subsets of species are merged and a first, comprehensive skeletal mechanism is created.

Such a merging results in the addition of more species to each investigated point: this unavoidably changes the performance of the final mechanism in the single points, most often by decreasing the local error. Therefore, a further step is carried on. The mechanism just obtained undergoes the sensitivity analysis as introduced by Zheng et al. for DRGASA [16]. As before, species with a value of $\tilde{R}_i$ higher than a fixed threshold are excluded from this procedure, and the same is done for F_i. The removal ranking is generated by evaluating the maximum error on the ignition delay time on the whole $T - P - \Phi$ space:

$$E_i = \max_{T-P-\Phi} \frac{|\tau_{ign,i} - \tau_{DRGEP,i}|}{\tau_{DRGEP,i}} \tag{9}$$

This ranking is then updated every n removals, with n depending on the size of the original mechanism and the computational availability: in their work, Niemeyer and Sung [27] used a value of n equal to 1, but for the largest kinetic mechanisms (e.g. heavy n-alkanes [28] or fuel surrogates [29]) this may result in impractical computational times.

3. Extension of the traditional approach

The flux-sensitivity coupling has been successfully adopted for skeletal mechanism generation in the past decade. Nevertheless, their focus on fuel and oxidizer as target species, and ignition delay as target property is not a guarantee of accuracy in all those phenomena and timescales not directly related to them. The main weaknesses can be summarized in these two points:

- As pointed out by Lu and Law [30], a reduction algorithm should provide *a priori* error control in such a way to guarantee the accuracy of the reduced mechanism. When reduction is species-targeted, controlling error on the fly while performing DRGEP reduction is not an easy task, since it would require error quantification in ideal reactors set up in the operating space. Therefore, unless a proper methodology

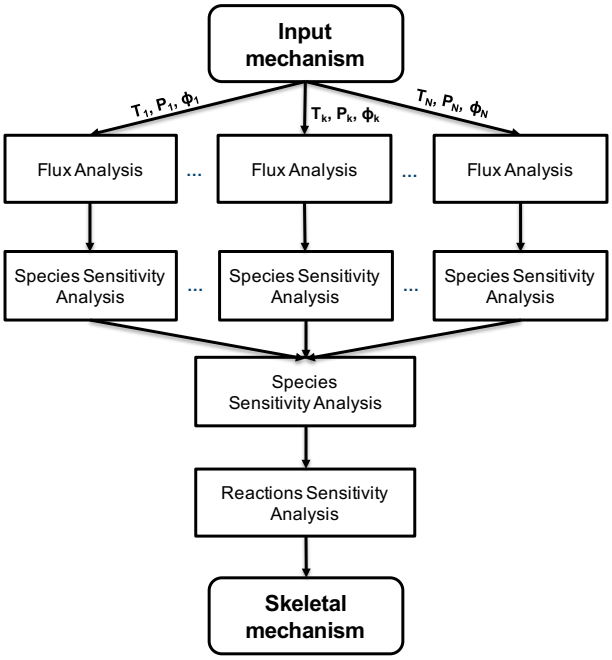

Figure 1: *Divide-and-conquer* structure of the reduction procedure

is developed, error control can then only be done *a posteriori.*

- Similarly, sensitivity analysis is not applicable in the described form, since it uses a single value, i.e. ignition delay, to summarize the importance of a species in the overall accuracy of the mechanism. When targets like the formation of a given species is to be retained (which cannot be represented by a single point), a different approach must be devised.

These considerations brought to the extension of the reduction methodology through two additional steps, which are described in detail in this Section. Combined to the framework already described, they provided a comprehensive procedure which allows to retain accuracy on the desired properties in the final mechanism. Such a procedure is described in the rest of this Section, and is graphically summarized in Figure 1.

3.1. Sensitivity analysis on species formation

The underlying principle of the approach described in Section 2.2 was extended in the context of a Species-Targeted Sensitivity Analysis. As a first step, DRGEP reduction is

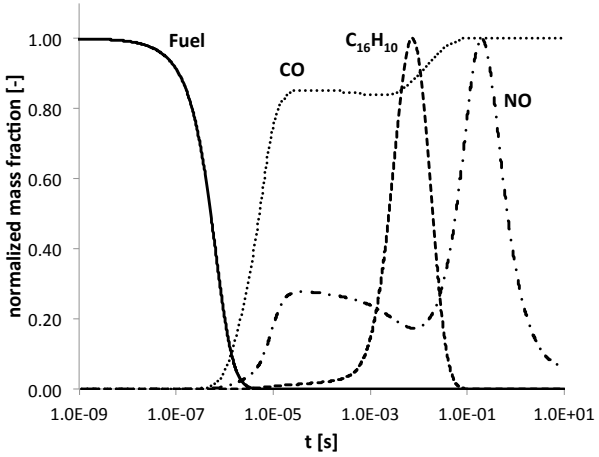

Figure 2: Mass fraction evolution of sample species over time, as detected in an isothermal plug flow reactor. Fuel = C_3H_8. Oxidizer: air. T = 1900 K. P = 1 atm. $\phi = 2$. The simulation was carried out using the POLIMI [31] mechanism (version 1412).

carried out in each sampled point, using the desired target species for the evaluation of coefficients in (1). As in Section 2.1, a threshold to $\tilde{R}_i$ (6) (10^{-3} or lower) is fixed, and the species with a lower value are removed from the local mechanisms. Afterwards, the marginal species to be analyzed are selected for each point by fixing an upper threshold to $\tilde{R}_i$. Here, the focus is then directed to the dynamics of formation of the considered species in the considered time scales. A lower and an upper reference time scales are selected according to species typical lifetime (Figure 2), and for each reactor the target molar fraction is obtained as a function of the logarithm of the reactor time. The same profiles are then obtained through the one-by-one removal of the marginal species. Each of them is compared to the reference curve through a functional data analysis [32]. A functional estimation of such profiles is carried out: in principle, this can be done in a wide variety of methods (e.g. smoothing splines), but since the profiles are the result of a numerical integration, the absence of experimental noise and the high number of available points justify the choice of a linear interpolation between adjacent points to obtain such a functional. Once the functional estimation has been performed for both the reference profile f and the tested curve g, the dissimilarity between them is evaluated through two indices:

$$\varepsilon_D(f,g) = \frac{\|f-g\|_{L^2}}{max\left(\|f\|_{L^2}, \|g\|_{L^2}\right)} \tag{10}$$

$$\varepsilon_S(f,g) = \frac{1}{2}\left\| \frac{f}{\|f\|_{L^2}} - \frac{g}{\|g\|_{L^2}} \right\|_{L^2} \tag{11}$$

where ε_D is the the normalized L^2-distance of the two functions f and g, and ε_S is the measure of the similarity between the two curves, in terms of the cosine of the angle between f and g. The formulations of (10) and (11) binds both the indices in assuming values between 0 and 1.

ε_D is basically the integral of the Residual Sum of Squares, normalized by the maximum L^2-norm. Yet, in presence of large plateaux (where $f \neq 0$ and $f' = 0$), its value becomes sensitive to the choice of upper and lower boundaries. Figure 3 shows two typical cases where it can occur. Here, CH_4 and CO_2 profiles obtained through the simulation of an adiabatic batch reactor were artificially shifted to obtain the dashed lines, and the error indexes (10) and (11) were calculated. In the first case (Figure 3a), moving the lower boundary from 10^{-7} to 10^{-6} s would result in an increase of ε_D from 0.237 to 0.300. Similarly, in Figure 3b, changing the upper boundary from 10^{-1} to 10^{-3} s would increase ε_D from 0.257 to 0.336.

Conversely, the value of ε_S in insensitive to boundary shifts, as long as they occur in the flat regions. Moreover, ε_S is insensitive to vertical dilatations:

$$\varepsilon_S(f,g) = \varepsilon_S(f, a \cdot g) \tag{12}$$

where a is a scalar. Figure 4 shows two related examples: the mass fraction profiles of $C_{16}H_{10}$ and NO obtained through the simulation of an isothermal batch reactor were vertically dilated to obtain the dashed lines. As a result, the value of ε_S is zero in both cases, while ε_D is affected by such a transformation and is then higher than zero.

Since the two indices evaluate different aspects of the comparison between each pair of profiles, a species ranking cannot be created in a straightforward way through a simple summation of them. Rather, in this work a species ranking is created through a statistical analysis of the indices resulting from the one-by-one removal procedure of the marginal species. For each reactor, the median and median absolute deviation (MAD) of ε_D and

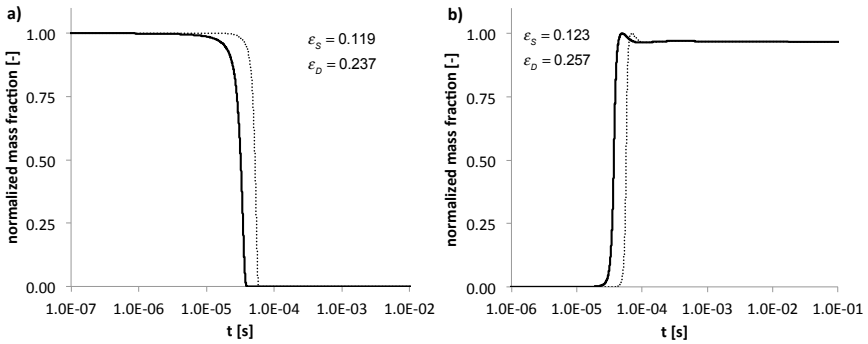

Figure 3: Time history of a) CH_4 and b) CO_2 in an adiabatic batch reactor. T = 1900 K. P = 1 atm. $\Phi = 2$. Continuous lines: original profiles. Dashed lines: profiles shifted in the x direction ($dt = 2 \cdot 10^{-5}\, s$). The simulation was carried out using the POLIMI_1412 [31] mechanism.

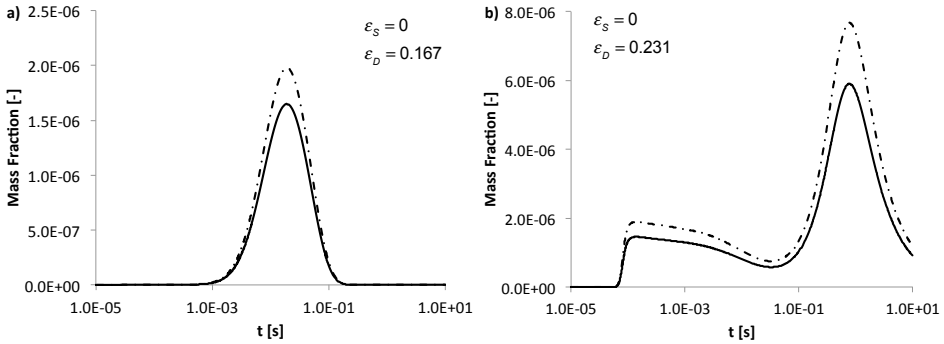

Figure 4: Time history of a) $C_{16}H_{10}$ and b) NO in an isothermal batch reactor. T = 1800 K. P = 1 atm. $\Phi = 2$. Continuous lines: original profiles. Dashed lines: profiles multiplied by a factor a) 1.2 and b) 1.3. The simulation was carried out using the POLIMI_1412 [31] mechanism.

ε_S are evaluated. For each i-th species, both indices are converted in terms of normalized deviations from the median value:

$$\hat{\varepsilon}_{D_i} = \frac{\varepsilon_{D_i} - \tilde{\varepsilon}_D}{MAD_D} \tag{13a}$$

$$\hat{\varepsilon}_{S_i} = \frac{\varepsilon_{S_i} - \tilde{\varepsilon}_S}{MAD_S} \tag{13b}$$

where $\tilde{\varepsilon}_D$ and $\tilde{\varepsilon}_S$ are the median values of all the tested models, and MAD is related to considered errors subset. The normalized values for distance and similarity indices are then summed up and the species ranking is then created.

With the same methodology described in Section 2.2, the species are removed one-by-one from the subsets related to each k-th reactor. The local error values are monitored for each removal, and the procedure is carried on for each reactor while both indices are lower than defined threshold values:

$$\varepsilon_{D_k} < \check{\varepsilon}_D \tag{14a}$$

$$\varepsilon_{S_k} < \check{\varepsilon}_S \tag{14b}$$

After completing the procedure for each point, the species subsets are merged, and an overall sensitivity analysis on species is carried out considering the whole $\mathrm{T-P-\Phi}$ range. Similarly, the removal ranking is created by taking the maximum indices over the $\mathrm{T-P-\Phi}$ range:

$$E_{D_i} = \max_{T-P-\Phi} \varepsilon_{D_i} \tag{15a}$$

$$E_{S_i} = \max_{T-P-\Phi} \varepsilon_{S_i} \tag{15b}$$

The normalized deviations of (15a) and (15b) are calculated as in (13a) and (13b), and the removal is carried on while the conditions (14a) and (14b) are valid on the whole range:

$$\max_{T-P-\Phi} (\varepsilon_{D_k}) < \check{E}_D \tag{16a}$$

$$\max_{T-P-\Phi} (\varepsilon_{S_k}) < \check{E}_S \tag{16b}$$

where $\check{E}_D$ and $\check{E}_S$ are two user-defined threshold values.

3.2. Sensitivity analysis on reactions

The use of sensitivity analysis to identify and understand the governing parameters in numerical combustion models has been of primary importance since the early 80s [11, 33–36]. Nowadays, the advancements in computing technology and numerical techniques have allowed its application also in systems with a very large number of involved parameters. Detailed kinetic models with thousands of reactions, like those involving heavy n-alkanes, belong to this group. In the case of kinetic models, the first-order sensitivity coefficients can be calculated with respect to the pre-exponential factor, activation energy or the whole kinetic constant if it does not change during the simulation. To the purposes of this work, sensitivity coefficients of pre-exponential factors are evaluated. The equations for sensitivity coefficients are derived from the ODE system representing the ideal reactor:

$$\begin{cases} \frac{d\mathbf{y}}{d\xi} = f\left(\mathbf{y}, \xi, \boldsymbol{\alpha}\right) \\ \boldsymbol{y}\left(\xi_0\right) = \boldsymbol{y_0} \end{cases} \tag{17}$$

where $\boldsymbol{y}$ is the vector of variables (mass fractions + temperature), ξ the independent variable (time in this case) and $\boldsymbol{\alpha}$ the vector of parameters, whose values control the evolution of the system. For unsteady systems like those under investigation, the sensitivity coefficients of the i-th variable with respect to the j-th parameter are then defined as:

$$s_{ij}\left(\xi\right) = \frac{\partial y_i\left(\xi\right)}{\partial \alpha_j} \tag{18}$$

and in their (locally) normalized form:

$$\hat{s}_{ij} = \frac{\partial \ln y_i}{\partial \ln \alpha_j} = \frac{\partial y_i}{\partial \alpha_j} \cdot \frac{\alpha_j}{y_i} \tag{19}$$

The total number of sensitivity coefficients, therefore, is equal to the product of the number of variables N_E and the number of parameters (i.e. reactions) N_P and may then easily become huge for a detailed mechanism. For the sake of completeness, it is worth pointing out that the sensitivity coefficients of pressure-dependent reactions are calculated by summing the relative contributions of high- and low-pressure pre-exponential

factors. By differentiating the system (17) with respect to the parameters α_{ij}, an ODE system is obtained for each j-th vector of parameters:

$$\begin{cases} \frac{d\boldsymbol{s_j}}{d\xi} = \boldsymbol{J}\boldsymbol{s_j} + \frac{\partial \boldsymbol{f}}{\partial \alpha_j} & j = 1 \dots N_P \\ \boldsymbol{s_j}\left(\xi_0\right) = 0 \end{cases} \tag{20}$$

where $\boldsymbol{J}$ is the ODE system (17) Jacobian matrix, $\mathrm{J_{ij}} = \frac{\partial \mathrm{f_i}}{\partial \mathrm{y_j}}$, and $\mathbf{s_j}$ has the size of $\mathbf{y}$ (number of variables). These equations are added to the system (17), and are dependent on them (note: the opposite is not true). The resulting system can be extremely demanding from a computational point of view, because of the number of added equations. Nevertheless, proper simplifying assumptions can make this problem affordable. Further details on the adopted resolution strategies can be found in Cuoci et al. [37].

In order to decouple the importance of pressure-dependent reactions from the pressure profile itself, isobaric reactors are used for this evaluation. After the reactor is solved and sensitivity coefficients are collected throughout the whole reactor length, they can be analyzed to identify the reactions which can be neglected. If general reactivity is to be preserved, fuel and oxidizer may be set as target species and the related sensitivity coefficients can be investigated. In this case, this procedure could be a useful completion of the framework described in Section 2. Otherwise, if a particular species is of interest (Section 3.1), the related values are analysed. In any case, the methodology is common: a characteristic coefficient of the j-th reaction with respect to the i-th species is evaluated as the mean integral value of the absolute sensitivity profile over time:

$$\bar{s}_{ij} = \frac{\int_0^\tau \left|\tilde{s}_{ij}\left(\xi\right)\right| d\xi}{\tau} \tag{21}$$

where τ is the length of the batch reactor simulation. Once the coefficients are evaluated, the j-th reaction may be discarded if, for all the considered reactors, $\bar{s}_{ij}$ is lower than a defined threshold for all the target species. As a reference, it was observed that 10^{-3} can be considered as a conservative reference threshold to keep accuracy on the system reactivity, being the residence time equal to ignition delay time in this case. Of course, if all the reactions involving a species are classified as unimportant, the species itself can be removed, too.

3.3. Reactor type and dynamics of species

What has been discussed in Sections 3.1 and 3.2 is intrinsically applicable only when 0D, transient autoignition phenomena are concerned, while in the past, DRG and DRG-based approaches also considered PSRs for the evaluation of (1) [15, 19, 27]. Traditionally, flux analyses have always considered adiabatic reactors because the focus is uniquely directed on preserving the overall reactivity. Thus, since ignition delay is the only target, coupling mass and energy balances is the most appropriate way to reach that target. On the other hand, when the interest falls on the dynamics of formation of one (or more) species in the different timescales, like in this work, coupling mass and energy balance and investigating then adiabatic phenomena may be counterproductive. Indeed, the main danger could reside in masking low temperature phenomena, whose importance may become even competitive with the upper temperature ones in operating conditions dissimilar from adiabatic reactors, where they would be insignificant. A further example may be provided by the different mechanisms concurring to the formation of nitrogen oxides (NO_x), which is kinetically controlled: it occurs through two main pathways [38], known as thermal and prompt mechanism, although the NNH and N_2O pathways play an important role in some conditions [39, 40]. In particular, thermal mechanism is very sensitive to temperature, and the concentration of NO_x increases exponentially with it; moreover, the related time scales are of the order of the second. On the other hand, prompt mechanism is not so temperature-sensitive as thermal, but mostly depends on the hydrocarbon radicals in the first pyrolysis steps of the hydrocarbon chain; therefore, it is complete after milliseconds. If adiabatic simulations are used for mechanism reduction in the presented framework, the formation of NO_x via prompt mechanism would be overcome by thermal, once ignition has occurred, and the adiabatic flame temperature has been reached. As a result, the obtained mechanism would be able to replicate such trends in autoignition phenomena, but not in more complex systems, where ignition is not the only involved phenomenon, and mixing conditions may not be ideal. Figure 5a shows the time-dependent formation of nitrogen oxides in an adiabatic batch reactor in fuel-rich conditions. It is possible to distinguish the two different mechanisms leading to NO formation and the final reduction of NO in rich conditions due to the reburning mechanism [2]. Yet, the quantitative formation of NO via the prompt path is quantita-

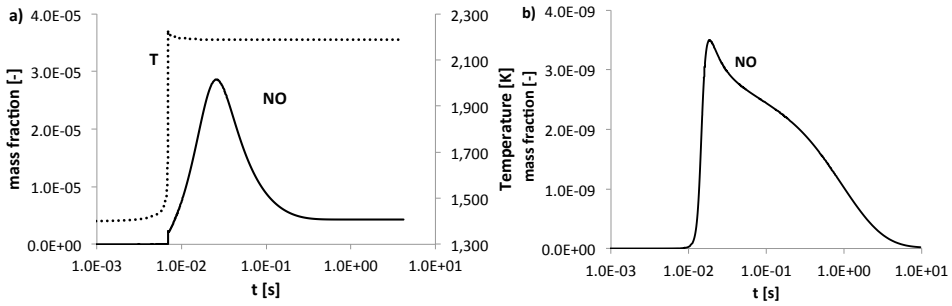

Figure 5: Time history of NO mass fraction in a) adiabatic (with temperature profile) and b) isothermal batch reactor. Fuel = CH_4. Oxidizer: air. T_0 = 1400 K. P = 1 atm. $\Phi = 3$. The simulation was carried out using the POLIMI_1412_NOx [31] mechanism.

tively much lower (5 - 10%) than the maximum amount, since the temperature rise due to ignition increases the importance of thermal mechanism, which ultimately overwhelms the former.

On the other hand, when isothermal reactors are adopted, the decoupling between mass and energy balance provides a clear overview of time scales and relative importance of the different mechanisms for an assigned set of initial conditions. Figure 5b shows the formation of nitrogen oxides in an isothermal batch reactor, with the same starting conditions as Figure 5a. As expectable, in the sampled conditions the prompt mechanism is the only formation path present, due to the high activation energy of the thermal one.

3.4. Software implementation

The strategy described in Sections 2 and 3 and illustrated in Figure 1 was implemented into `DoctorSMOKE++`, a numerical code based on the open-source software `OpenSMOKE++` [37], on turn a C++ framework for the numerical simulation of reacting flows with detailed kinetic mechanisms. `OpenSMOKE++` allows the resolution of the numerical models of 0D Reactors (batch, perfectly stirred, plug flow, shock tube reactors) as well as more complex models like premixed and counterflow 1D flames. It includes interfaces for several open source libraries for the resolution of the related ODE systems, and it also implements its own in-house solver. `DoctorSMOKE++` supports the MPI standard for parallel computing, and will be freely available (for academic purposes) for Linux, Mac OS X and Windows systems after the publication of this paper on `http://creckmodeling.chem.polimi.it`.

4. Applications

The effectiveness of the proposed procedure is here demonstrated through two case studies: Section 4.1 presents the sample development of a mechanism of a Gasoline surrogate for the CFD simulation of Internal Combustion (IC) Engines. It was derived with ignition delay time as reduction target, thus following the improved flux-sensitivity procedure proposed in Section 2, and further completed by the Sensitivity Analysis on reactions introduced in Section 3.2. Then, Section 4.2 describes the development of two skeletal models for methane combustion, with NO_x kinetics as reduction target. Here, the approaches described in Sections 3.1 and 3.2 are successfully applied. All the mechanisms are available as supplemental material.

4.1. Toluene Reference Fuel mechanism

The use of single-component fuels is often too simplistic to mimick all the physico-chemical properties of interest in transportation fuels (i.e. flash point, autoignition temperature, octane and cetane numbers, etc.). For this reason, the use of multicomponent surrogates to reproduce the combustion behavior of transportation fuels has been gaining increasing interest in the latest twenty years. Extensive research is being carried out on this topic: the state of the art was recently reviewed by Pitz and Mueller [41].

In the present work a skeletal mechanism for a gasoline surrogate was developed. For the ideal reactor calculations, the starting composition was chosen following Gauthier et al. [42], who selected a 63/20/17 mixture (in mole fractions) of *n*-heptane, iso-octane and toluene as reference composition of *RD387* gasoline. Such a gasoline was the reference for the development of the related LLNL model by Mehl et al. [29]. 81 adiabatic, constant volume batch reactors were used to the purpose, distributed in the operating space indicated in Table 1. A higher sampling thickness was chosen in the low-temperature region due to its higher sensitivity of reactivity to temperature variations.. Table 2 lists the progressive mechanisms obtained through `DoctorSMOKE++`. Skeletal mechanisms were built up with a target of 15% maximum error on the final ignition delay (the average value in sensitivity-based approaches [19, 27] is between 10 and 30%). An intermediate threshold of 7.5% was chosen for the DRGEP phase. Maximum and average errors on

	Range
Temperature	600 K − 1800 K
Pressure	1 atm − 50 atm
Equivalence ratio	0.5 − 2

Table 1: POLIMI *RD387:* Operating conditions used for reduction.

Version	Species	Reactions	Max Error %	Mean Error %
POLIMI_1407	451	17848	-	-
DRGEP	196	6646	3.2	1.4
Sensitivity Analysis	115	1939	15.7	6.2
Reactions Sensitivity	115	856	15.8	5.4

Table 2: POLIMI *RD387* kinetic models: size of detailed and progressively reduced mechanisms, and related errors.

the ignition delay are defined as:

$$\varepsilon_{max} = \max_{T,P,\Phi} (\varepsilon_k) \tag{22}$$

$$\bar{\varepsilon} = \frac{\sum_{i=1}^{n} \varepsilon_k}{n} \tag{23}$$

where n is the number of reactors. Starting from the complete POLIMI mechanism [31] (version 1412), a final mechanism of 115 species and 856 reactions was obtained. Details about error distribution are provided in Figure 6. The mechanism behaves quite satisfactorily in predicting the properties of pure components. The laminar flame speed of gasoline surrogate was calculated with a starting equivolume liquid mixture of n-heptane, iso-octane and toluene (i.e. a 30.4/27.2/42.4 mixture in mole fractions) following the indications of Sileghem et al. [43]. In that work, the authors derived it through a mixing rule based on the energy fraction, and successfully mimicked the experimental values of the investigated gasoline. Figure 7 shows such an evaluation through detailed and skeletal mechanism. The agreement between the two curves is almost complete, but the tested mechanism also behaved well for the three pure components. This results in a high flexibility of the obtained model, which can then represent TRFs with a different composition from what used for reduction.

In spite of the increasing importance owned by surrogate models, the development of dedicated skeletal mechanisms is still an almost uncharted territory: starting from

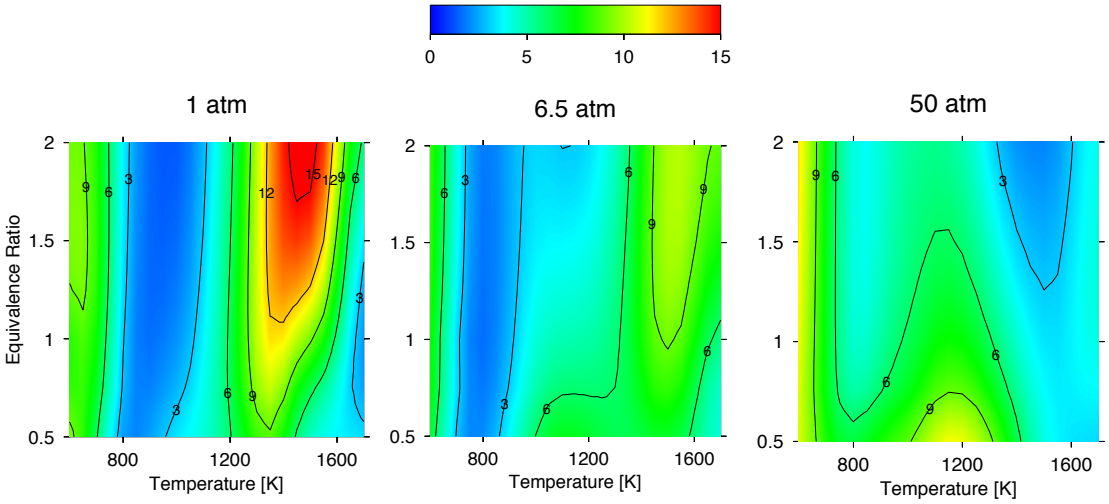

Figure 6: POLIMI *RD387* mechanism (115 species) error maps: comparison at low, intermediate and high pressures.

the LLNL mechanism for gasoline surrogates [29], Niemeyer and Sung [27] obtained a 233-species skeletal model for a TRF mechanism operating in conditions typical of Homogeneous Charge Compression Ignition, and a 97-species mechanism for a TRF fuel operating in Spark Ignition or Compression Ignition engines. From the same mechanism, Mehl et al. [49] developed a 312-species skeletal mechanism for a gasoline surrogate operating in lean conditions, typical of HCCI engines. Luong et al. [50] obtained a 171-species model for lean Primary Reference Fuel/air mixtures from the related LLNL mechanism [51]. This was then further reduced to 116 species through quasi steady-state approximation [52] for its use in Direct Numerical Simulations. More recently, Cai and Pitsch [53] developed an optimized chemical mechanism for PRF/toluene mixtures, consisting of 314 species and 2327 chemical reactions, obtained through a combination of LLNL PRF mechanism [51] and the model of Narayanaswamy et al. [54]. For the sake of completeness, a performance comparison between these mechanisms and the POLIMI skeletal developed in this work is reported in the supplemental material.

Actually, the smaller dimensions of the model obtained here benefits from the structure of the original one, too. Indeed, POLIMI mechanism is built up following an upstream lumping approach [55], thanks to which the starting dimensions are significantly

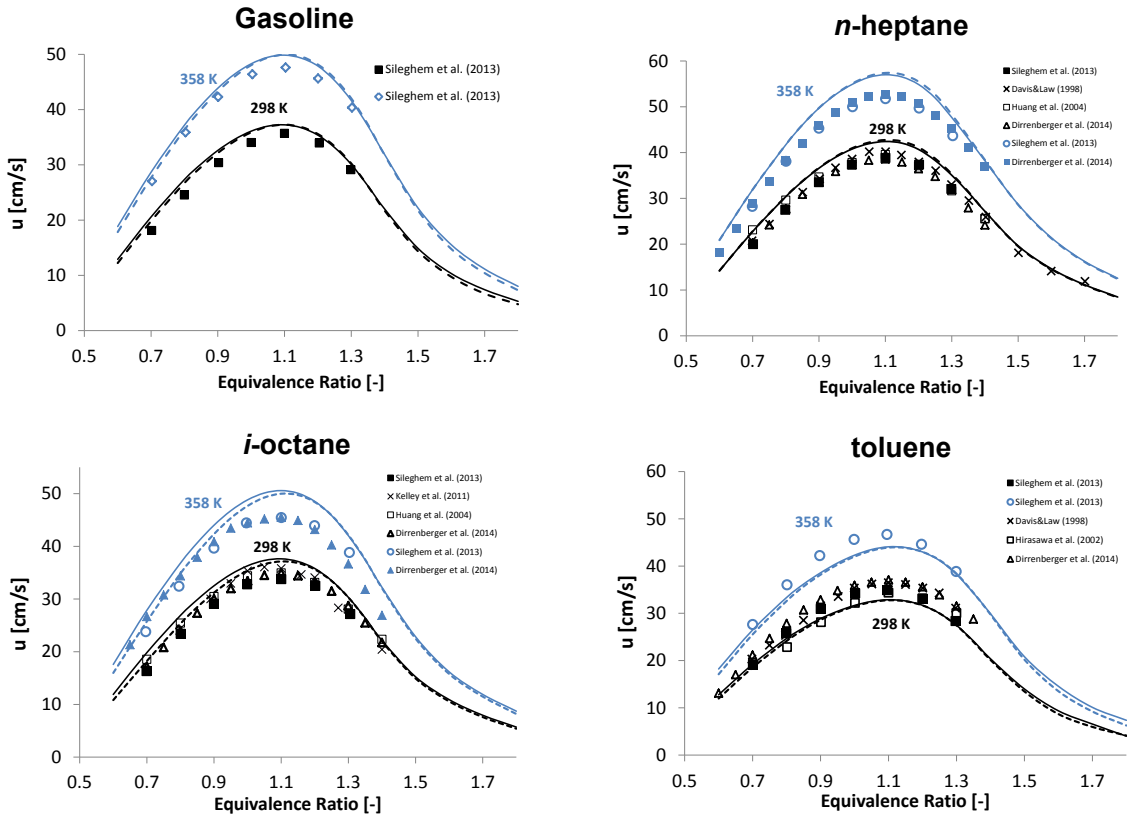

Figure 7: Laminar flame speeds of gasoline surrogate (1/3 n-heptane, 1/3 i-octane, 1/3 toluene in volume fractions) and pure components. Continuous lines: detailed model. Dashed lines: POLIMI *RD387* skeletal model. Experimental data from [43–48].

	Range
Temperature	800 K − 1800 K
Pressure	1 atm
Equivalence ratio	0.5 − 2

Table 3: POLIMI CH_4/NO_x mechanism: Operating conditions used for reduction

lower than a full model, like the one used by Mehl et al. [49] in their work (about 1550 species and 6000 reactions), without sacrificing accuracy though. Recently, several attempts of coupling lumping and skeletal reduction were carried out [27, 56–58]. Yet, the use of lumping and skeletal reduction in this right order proved more effective, as previously discussed by Ranzi et al. [59].

Finally, it is also worth pointing out the numerical improvements of the created framework: by performing the same reduction process with a combination of classical DRGEP and sensitivity analysis with the same 15% final threshold of error on ignition delay time, a mechanism with 132 species and 972 reactions was obtained in 7.1 hours on a parallel cluster, using 24 cores (Intel Xeon X5675 – 3.07 GHz). Therefore, considering that the reduction with `DoctorSMOKE++` required 5.3 hours, a twofold benefit was obtained, both on time and convergence, and the time savings of carrying out a divide-and-conquer procedure overcome the computing demand required by a repeated calculation of species ranking in sensitivity analysis.

4.2. CH_4/NO_x skeletal mechanism

The development and validation of a mechanism for methane combustion with the inclusion of NO_x formation are now addressed. Literature examples of skeletal mechanisms obtained *ad hoc* through an error control on specific species are very scarce; the only example can be found in the work by Nagy and Turanyi [13], based on a Simulation Error Minimization approach. Above all, automatically reduced models for species not directly dependent on autoignition have not been obtained to the authors' knowledge. Rather, in the past a decoupling methodology has been adopted, consisting in removing upstream the sub-model of interest, applying the classical flux/sensitivity analysis approach, and merging the two subsets at the end [60].

In this work, reduction is carried out on isothermal, constant pressure batch reactors, as motivated in Section 3.3. The operating space is defined in Table 3. As starting

ID	$\check{E}_D$	$\check{E}_S$	Core mech		NO sub-mech		Final mech	
			Species	Reactions	Species	Reactions	Species	Reactions
1	0.15	0.05	27	181	60	623	59	459
2	0.3	0.1			55	490	55	400

Table 4: Accuracy and size of the two NO_x mechanisms obtained in this work.

mechanism, the POLIMI detailed model for NO_x was adopted (version 1412), made up of 148 species and 3211 reactions, which includes hydrocarbon fuels up to 3 carbon atoms. STSA reduction was carried out after the traditional procedure, in order to preserve ignition characteristics. By using a maximum error on ignition delay equal to 15%, a core mechanism of 27 species and 181 reactions was generated after sensitivity analysis on ignition delay. By using NO as target species, the threshold values of ε_D and ε_S were selected at two different levels. Two subsequent mechanisms were obtained, which were merged with the core model previously obtained. The sensitivity analysis on reaction parameters described in Section 3.2 was applied by using CH_4, O_2 and NO as target species. The final dimensions are indicated in Table 4.

Interestingly, the size of the most accurate mechanism decreased after merging. This is not surprising, though, and is due to the strong coupling between species affecting kinetic mechanisms. As a consequence, the progressive, one-by-one removal process implemented in this framework may retain a species A, whose importance in the final target is significant only when coupled with another species B. It may happen, then, that B is removed and the importance of A becomes then negligible; this cannot be detected by the algorithm because the decision of retaining A had already been made. Anyhow, this issue is fixed by the sensitivity analysis on reactions, which finds downstream a negligible value of sensitivity coefficients of all the reactions where A is involved, and discards it at the end of the process.

The four species constituting the difference between the two mechanisms are the carbon radical (C), acetyl radical (C_2H), propane (C_3H_8) and isocyanate radical (NCO). They could not be detected through a decoupling methodology, since they do not belong to the 27-species core subset (3 of them do not even contain nitrogen), but necessarily needed an NO-targeted analysis to properly account for their importance in the considered operating conditions.

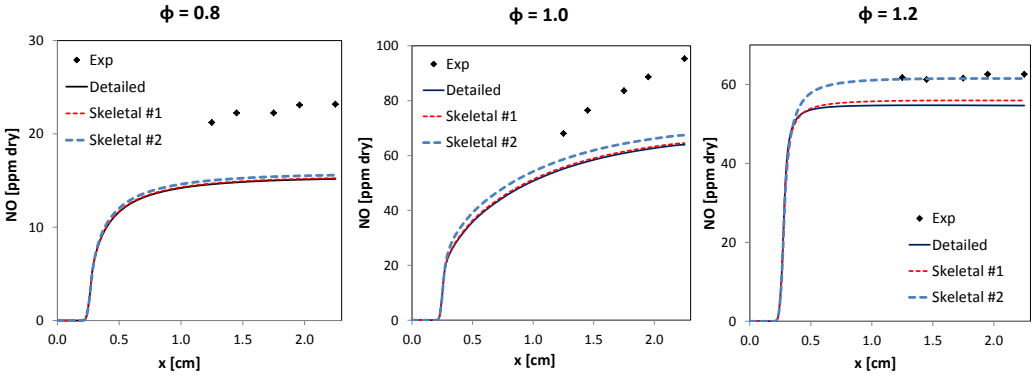

Figure 8: NO formation in a laminar premixed flame (CH_4/Air). Experimental data by Konnov et al. [61].

The obtained mechanisms underwent an extensive validation through comparison with experimental data and detailed mechanism output in several case studies. Based on the operating conditions adopted by Konnov et al. [61], the NO concentrations in the postflame zone of a laminar premixed CH_4/air flame were calculated. The equivalence ratio was varied between 0.8 and 1.2, and 3 axial profiles are shown in Figure 8. A good agreement between detailed and reduced mechanism can be observed, with the highest relative error amounting to ~15% in the worst case. The largest errors are observed at a high equivalence ratio.

Similarly, the NO formation in a CH_4/H_2/air flame was calculated, by reproducing the experimental tests carried out by Coppens et al. [62]. Figure 9 summarizes the obtained numerical results. If the overlapping between curves in the laminar flame speed evaluation confirms the reliability of the core mechanism and its ability to correctly reproduce the overall reactivity, the NO profiles as a function of the equivalence ratio are much more interesting for the purposes of this work: both numerically and experimentally, a double peak in NO formation, respectively at about $\Phi = 1.05$ and $\Phi = 1.35$ is observed. This is due to the competition between the two pathways, which bring to the formation of NO. The first maximum corresponds to the highest temperature of the burning flame, reached in proximity of stoichiometric ratio: here, the thermal path prevails. On the other hand, the prompt pathway is emphasized in fuel-rich mixtures [38], this resulting in the second maximum. In both cases, the skeletal model well predicts such behaviors, with a slight

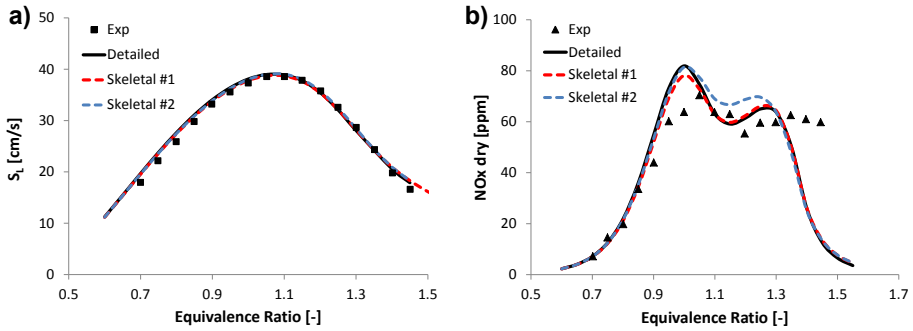

Figure 9: NO formation in a laminar premixed flame (85% CH_4/ 15% H_2 in air). a) Laminar Flame speed. b) NO concentration (dry) evaluated at 10 mm. Experimental data by Coppens et al [62].

overprediction of the prompt-related maximum, which is coherent with what observed in the test case of Konnov et al. A drop in the NO prediction is observed at highest equivalence ratios with both mechanisms, and the same behavior was also observed in the experimental work [62]. Although this is not related to mechanism reduction and is then beyond the scope of this work, it is worth mentioning that Coppens and coworkers explained such a behavior to buoyancy effects, which would lead to an exchange of oxygen between the burnt gases and the surrounding air. This would allow the continuation of the prompt NO mechanism, even at higher equivalence ratios, where the reduction of NO to N_2 becomes important.

A further validation of the skeletal mechanisms was carried out through the investigation of laminar counterflow diffusion flames. In addition to being complementary to the premixed flames already analysed, a high interest in this setup is motivated by the theoretical foundations of flamelet-based models of turbulent combustion [63], through which turbulent flow and mixture fields are solved separately from chemistry. Literature shows how they were successfully applied for the prediction of nitrogen oxides in turbulent, nonpremixed flames [64, 65]. In the recent past, several counterflow configurations for the analysis of NO emissions have been investigated [66–68]. In this work, the two experimental measurements carried out by Shimizu et al. [66] were reproduced with both the detailed and the skeletal models. The fuel stream was a mixture of 70% CH_4 and 30% N_2 in the first experiment, 100% CH_4 in the second. Air was used as oxidizer in both experiments. Table 5 summarizes the operating conditions. It is worth pointing

#	T_{fuel} $[K]$	T_{ox} $[K]$	P $[atm]$	v_{fuel} $[cm/s]$	v_{ox} $[cm/s]$	d $[cm]$	a_c $[1/s]$
1	300	300	1	15.2	12.5	1	50
2	300	300	1	70	70	1.5	163

Table 5: Counterflow flame setup of CH_4/Air flames in the reproduced experiments [66].

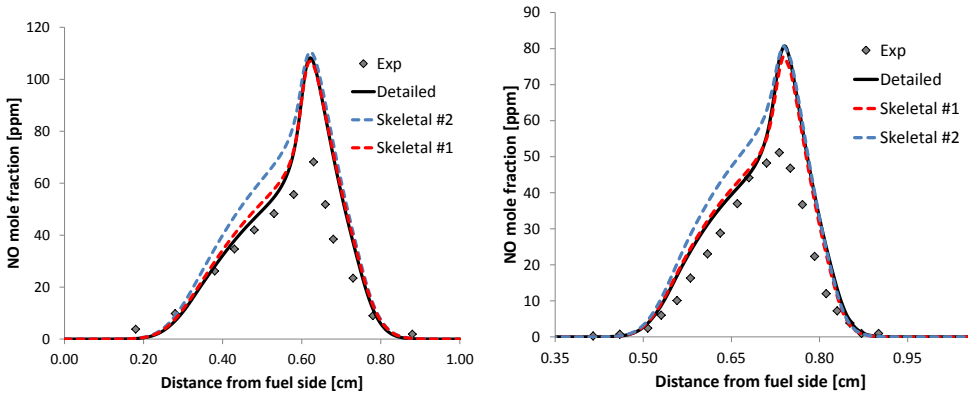

Figure 10: NO formation in laminar counterflow flames. Experimental data by Shimizu et al. [66].

out that in the considered flames the prompt mechanism is dominant because of the low temperatures.

A satisfactory agreement between the detailed and skeletal profiles can be found. In particular, the peak value is well caught by the skeletal mechanism, with a maximum error of about 2-5 %. Therefore, accuracy on prompt sub-mechanism is satisfactorily retained, as it had been partially shown in the previous assessments, too.

Further validation of the mechanism is not reported here for the sake of compactness, but is available as supplemental material.

Conclusions

This work has been focused at extending the established kinetic reduction techniques, towards the generation of skeletal models able to keep the desired accuracy on the targeted species, whose time scales are not directly connected to ignition phenomena. To this purpose, the sensitivity analysis phase of the DRGASA [16] and DRGEPSA [19] reduction frameworks was extended by shifting its focus from the ignition delay time (a single point) to the whole dynamics of formation of the considered species (a curve). This

required the development of a proper metric to evaluate the difference (i.e. the error) between species profiles. Two indices were introduced, describing distance and similarity between curves. A statistical combination between them allowed to obtain a species ranking, and to progressively remove them from the original mechanism, until reaching the desired degree of accuracy. Downstream of it, a sensitivity analysis on reactions was implemented, through the development of an additional index, assessing the importance of each reaction in the formation of the targeted species, thus allowing the elimination of the unimportant ones. These two extensions were then followed by general improvements to the whole reduction approach, both numerical and conceptual:

i. Split of sensitivity analysis into a local, *divide-and-conquer* research of the minimum number of species in the $T-P-\Phi$ space, followed then by a range-wide procedure. Considering that this is the most demanding part of the algorithm, a significant overall speedup can then be obtained.
ii. Introduction of a restart factor ρ, i.e. a dynamic recalculation of species ranking when seeking the local minimum.
iii. Improvement on the selection of marginal species when carrying out sensitivity analysis on ignition delay time, through an additional criterion based on production and consumption rates.

The combination of such improvements resulted in a a better convergence of the presented framework than traditional flux-sensitivity analysis, which could be obtained in lower computing times, too. To prove its efficacy, two applications of the overall procedure were carried out. A chemical mechanism for a gasoline surrogate, for engine applications, was developed, based on the reference composition indicated by Gauthier et al. [42]. Made up of 115 species and 856 reactions, it was successfully validated through autoignition delay times and laminar flame speed evaluation of both gasoline surrogate and pure components. Then, the whole methodology was applied to develop a skeletal model for CH_4 combustion with the inclusion of NO chemistry. The smallest obtained mechanism resulted in 55 species and 400 reactions, and it was shown how it can reasonably replace the original mechanism in the targeted operating range, well predicting the thermal and prompt formation paths.

The described methodology can be used for the attainment of *ad hoc* models of a wide range of pollutant compounds: not only nitrogen oxides (NO_x), but also sulphur oxides (SO_x) and chlorinated compounds. In particular, it can be applied to PAHs, too, thus providing a reliable gas-phase model for the prediction of soot formation, which is currently treated with several different methodologies [69–72]. Such a coupling will be the subject of future research.

Acknowledgements

The authors would like to acknowledge the active contribution of Mara Bernardi (Department of Mathematics, Politecnico di Milano) for her precious suggestions about functional data analysis. The role of Loris Vernier and Matteo Pelucchi (Politecnico di Milano) in the development and validation of the NO_x detailed mechanism is also fully recognized. Finally, the free concession of the MARS [19] software by Kyle Niemeyer, PhD (Oregon State University) is gratefully acknowledged.

Supplemental Material

Supplementary data associated with this article can be found, in the online version, at doi:XXX.

References

[1] C. S. McEnally, L. D. Pfefferle, B. Atakan, K. Kohse-Höinghaus, Studies of aromatic hydrocarbon formation mechanisms in flames: Progress towards closing the fuel gap, Progress in Energy and Combustion Science 32 (3) (2006) 247–294.

[2] A. Frassoldati, T. Faravelli, E. Ranzi, Kinetic modeling of the interactions between NO and hydrocarbons at high temperature, Combustion and Flame 135 (1) (2003) 97–112.

[3] S. H. Won, B. Windom, B. Jiang, Y. Ju, The role of low temperature fuel chemistry on turbulent flame propagation, Combustion and Flame 161 (2) (2014) 475–483.

[4] G. Ribert, K. Wang, L. Vervisch, A multi-zone self-similar chemistry tabulation with application to auto-ignition including cool-flames effects, Fuel 91 (1) (2012) 87–92.

[5] S. Sarathy, C. Westbrook, M. Mehl, W. Pitz, C. Togbe, P. Dagaut, H. Wang, M. Oehlschlaeger, U. Niemann, K. Seshadri, et al., Comprehensive chemical kinetic modeling of the oxidation of 2-methylalkanes from C_7 to C_{20}, Combustion and flame 158 (12) (2011) 2338–2357.

[6] T. Lu, C. K. Law, Toward accommodating realistic fuel chemistry in large-scale computations, Progress in Energy and Combustion Science 35 (2) (2009) 192–215.

[7] T. Turányi, A. S. Tomlin, Analysis of Kinetic Reaction Mechanisms, Springer, 2014.

[8] H. Wang, M. Frenklach, Detailed reduction of reaction mechanisms for flame modeling, Combustion and Flame 87 (3) (1991) 365–370.

[9] H. Rabitz, M. Kramer, D. Dacol, Sensitivity analysis in chemical kinetics, Annual review of physical chemistry 34 (1) (1983) 419–461.

[10] A. S. Tomlin, M. J. Pilling, J. H. Merkin, J. Brindley, N. Burgess, A. Gough, Reduced mechanisms for propane pyrolysis, Industrial & engineering chemistry research 34 (11) (1995) 3749–3760.

[11] N. J. Brown, G. Li, M. L. Koszykowski, Mechanism reduction via principal component analysis, International journal of chemical kinetics 29 (6) (1997) 393–414.

[12] S. Vajda, T. Turányi, Principal component analysis for reducing the Edelson-Field-Noyes model of the Belousov-Zhabotinskii reaction, The Journal of Physical Chemistry 90 (8) (1986) 1664–1670.

[13] T. Nagy, T. Turányi, Reduction of very large reaction mechanisms using methods based on simulation error minimization, Combustion and Flame 156 (2) (2009) 417–428.

[14] T. Turanyi, Reduction of large reaction mechanisms, New journal of chemistry 14 (11) (1990) 795–803.

[15] T. Lu, C. K. Law, A directed relation graph method for mechanism reduction, Proceedings of the Combustion Institute 30 (1) (2005) 1333–1341.

[16] X. Zheng, T. Lu, C. Law, Experimental counterflow ignition temperatures and reaction mechanisms of 1, 3-butadiene, Proceedings of the Combustion Institute 31 (1) (2007) 367–375.

[17] P. Pepiot-Desjardins, H. Pitsch, An efficient error-propagation-based reduction method for large chemical kinetic mechanisms, Combustion and Flame 154 (1) (2008) 67–81.

[18] W. Sun, Z. Chen, X. Gou, Y. Ju, A path flux analysis method for the reduction of detailed chemical kinetic mechanisms, Combustion and Flame 157 (7) (2010) 1298–1307.

[19] K. E. Niemeyer, C.-J. Sung, M. P. Raju, Skeletal mechanism generation for surrogate fuels using

directed relation graph with error propagation and sensitivity analysis, Combustion and flame 157 (9) (2010) 1760–1770.

[20] L. Liang, J. G. Stevens, J. T. Farrell, A dynamic adaptive chemistry scheme for reactive flow computations, Proceedings of the Combustion Institute 32 (1) (2009) 527–534.

[21] F. Contino, J.-B. Masurier, F. Foucher, T. Lucchini, G. D'Errico, P. Dagaut, CFD simulations using the TDAC method to model iso-octane combustion for a large range of ozone seeding and temperature conditions in a single cylinder HCCI engine, Fuel 137 (2014) 179–184.

[22] S. Pope, Computationally efficient implementation of combustion chemistry using in situ adaptive tabulation .

[23] Y. Xin, D. A. Sheen, H. Wang, C. K. Law, Skeletal reaction model generation, uncertainty quantification and minimization: Combustion of butane, Combustion and Flame 161 (12) (2014) 3031–3039.

[24] K. E. Niemeyer, C.-J. Sung, On the importance of graph search algorithms for DRGEP-based mechanism reduction methods, Combustion and Flame 158 (8) (2011) 1439–1443.

[25] E. W. Dijkstra, A note on two problems in connexion with graphs, Numerische mathematik 1 (1) (1959) 269–271.

[26] I. G. Zsély, T. Turányi, The influence of thermal coupling and diffusion on the importance of reactions: The case study of hydrogen–air combustion, Physical Chemistry Chemical Physics 5 (17) (2003) 3622–3631.

[27] K. Niemeyer, C.-J. Sung, Reduced chemistry for a gasoline surrogate valid at engine-relevant conditions, Energy and Fuels 29 (2) (2015) 1172–1185.

[28] C. K. Westbrook, W. J. Pitz, O. Herbinet, H. J. Curran, E. J. Silke, A comprehensive detailed chemical kinetic reaction mechanism for combustion of *n*-alkane hydrocarbons from *n*-octane to *n*-hexadecane, Combustion and Flame 156 (1) (2009) 181–199.

[29] M. Mehl, W. J. Pitz, C. K. Westbrook, H. J. Curran, Kinetic modeling of gasoline surrogate components and mixtures under engine conditions, Proceedings of the Combustion Institute 33 (1) (2011) 193–200.

[30] T. Lu, C. K. Law, C. S. Yoo, J. H. Chen, Dynamic stiffness removal for direct numerical simulations, Combustion and Flame 156 (8) (2009) 1542–1551.

[31] E. Ranzi, A. Frassoldati, R. Grana, A. Cuoci, T. Faravelli, A. Kelley, C. Law, Hierarchical and comparative kinetic modeling of laminar flame speeds of hydrocarbon and oxygenated fuels, Progress in Energy and Combustion Science 38 (4) (2012) 468–501.

[32] J. O. Ramsay, Functional data analysis, Wiley Online Library, 2006.

[33] J. A. Miller, M. C. Branch, W. J. McLean, D. W. Chandler, M. D. Smooke, R. J. Kee, The conversion of HCN to NO and N2 in H2-O2-HCN-Ar flames at low pressure, Symposium (International) on Combustion 20 (1) (1985) 673 – 684, ISSN 0082-0784.

[34] T. P. Coffee, J. M. Heimerl, Sensitivity analysis for premixed, laminar, steady state flames, Combustion and Flame 50 (1983) 323–340.

[35] Y. Reuven, M. D. Smooke, H. Rabitz, Sensitivity analysis of boundary value problems: Application to nonlinear reaction-diffusion systems, Journal of computational physics 64 (1) (1986) 27–55.

[36] R. Rota, F. Bonini, A. Servida, M. Morbidelli, S. Carra, Analysis of detailed kinetic schemes for combustion processes: Application to a methane-ethane mixture, Chemical engineering science 49 (24) (1994) 4211–4221.

[37] A. Cuoci, A. Frassoldati, T. Faravelli, E. Ranzi, OpenSMOKE++: An object-oriented framework for the numerical modeling of reactive systems with detailed kinetic mechanisms, Computer Physics Communications 192 (2015) 237–264.

[38] C. E. Baukal Jr, Industrial burners handbook, CRC press, 2004.

[39] E. Ranzi, A wide-range kinetic modeling study of oxidation and combustion of transportation fuels and surrogate mixtures, Energy & fuels 20 (3) (2006) 1024–1032.

[40] A. Frassoldati, A. Cuoci, T. Faravelli, E. Ranzi, S. Colantuoni, P. D. Martino, G. Cinque, Experimental and modeling study of a low NOx combustor for aero-engine turbofan, Combustion Science and Technology 181 (3) (2009) 483–495.

[41] W. J. Pitz, C. J. Mueller, Recent progress in the development of diesel surrogate fuels, Progress in Energy and Combustion Science 37 (3) (2011) 330–350.

[42] B. Gauthier, D. Davidson, R. Hanson, Shock tube determination of ignition delay times in full-blend and surrogate fuel mixtures, Combustion and Flame 139 (4) (2004) 300–311.

[43] L. Sileghem, V. Alekseev, J. Vancoillie, K. Van Geem, E. Nilsson, S. Verhelst, A. Konnov, Laminar burning velocity of gasoline and the gasoline surrogate components iso-octane, n-heptane and toluene, Fuel 112 (2013) 355–365.

[44] S. Davis, C. Law, Laminar flame speeds and oxidation kinetics of iso-octane-air and *n*-heptane-air flames, Symposium (International) on Combustion 27 (1) (1998) 521–527.

[45] Y. Huang, C. Sung, J. Eng, Laminar flame speeds of primary reference fuels and reformer gas mixtures, Combustion and Flame 139 (3) (2004) 239–251.

[46] P. Dirrenberger, P.-A. Glaude, R. Bounaceur, H. Le Gall, A. P. da Cruz, A. Konnov, F. Battin-Leclerc, Laminar burning velocity of gasolines with addition of ethanol, Fuel 115 (2014) 162–169.

[47] A. Kelley, A. Smallbone, D. Zhu, C. Law, Laminar flame speeds of C_5 to C_8 *n*-alkanes at elevated pressures: Experimental determination, fuel similarity, and stretch sensitivity, Proceedings of the Combustion Institute 33 (1) (2011) 963–970.

[48] T. Hirasawa, C. Sung, A. Joshi, Z. Yang, H. Wang, C. Law, Determination of laminar flame speeds using digital particle image velocimetry: Binary Fuel blends of ethylene, *n*-butane, and toluene, Proceedings of the Combustion Institute 29 (2) (2002) 1427–1434.

[49] M. Mehl, J.-Y. Chen, W. J. Pitz, S. Sarathy, C. K. Westbrook, An approach for formulating surrogates for gasoline with application toward a reduced surrogate mechanism for CFD engine modeling, Energy & Fuels 25 (11) (2011) 5215–5223.

[50] M. B. Luong, Z. Luo, T. Lu, S. H. Chung, C. S. Yoo, Direct numerical simulations of the ignition of lean primary reference fuel/air mixtures with temperature inhomogeneities, Combustion and Flame 160 (10) (2013) 2038 – 2047.

[51] H. J. Curran, P. Gaffuri, W. Pitz, C. Westbrook, A comprehensive modeling study of iso-octane oxidation, Combustion and flame 129 (3) (2002) 253–280.

[52] T. Lu, C. K. Law, Systematic approach to obtain analytic solutions of quasi steady state species in reduced mechanisms, The Journal of Physical Chemistry A 110 (49) (2006) 13202–13208.

[53] L. Cai, H. Pitsch, Optimized chemical mechanism for combustion of gasoline surrogate fuels, Combustion and Flame 162 (5) (2015) 1623 – 1637.

[54] K. Narayanaswamy, G. Blanquart, H. Pitsch, A consistent chemical mechanism for oxidation of substituted aromatic species, Combustion and Flame 157 (10) (2010) 1879–1898.

[55] E. Ranzi, M. Dente, A. Goldaniga, G. Bozzano, T. Faravelli, Lumping procedures in detailed kinetic modeling of gasification, pyrolysis, partial oxidation and combustion of hydrocarbon mixtures, Progress in Energy and Combustion Science 27 (1) (2001) 99–139.

[56] T. Lu, C. K. Law, Strategies for mechanism reduction for large hydrocarbons: n-heptane, Combustion and flame 154 (1) (2008) 153–163.

[57] K. Narayanaswamy, P. Pepiot, H. Pitsch, A chemical mechanism for low to high temperature oxidation of *n*-dodecane as a component of transportation fuel surrogates, Combustion and Flame 161 (4) (2014) 866–884.

[58] A. Stagni, A. Cuoci, A. Frassoldati, T. Faravelli, E. Ranzi, Lumping and reduction of detailed kinetic schemes: An effective coupling, Industrial and Engineering Chemistry Research 53 (22) (2014) 9004–9016.

[59] E. Ranzi, A. Frassoldati, A. Stagni, M. Pelucchi, A. Cuoci, T. Faravelli, Reduced Kinetic Schemes of Complex Reaction Systems: Fossil and Biomass-Derived Transportation Fuels, International Journal of Chemical Kinetics 46 (9) (2014) 512–542.

[60] T. Lu, C. K. Law, A criterion based on computational singular perturbation for the identification of quasi steady state species: A reduced mechanism for methane oxidation with NO chemistry, Combustion and Flame 154 (4) (2008) 761–774.

[61] A. Konnov, I. Dyakov, J. De Ruyck, Probe sampling measurements and modeling of nitric oxide formation in methane-air flames, Combustion science and technology 169 (1) (2001) 127–153.

[62] F. Coppens, J. De Ruyck, A. Konnov, Effects of hydrogen enrichment on adiabatic burning velocity and NO formation in methane + air flames, Experimental Thermal and Fluid Science 31 (5) (2007) 437–444.

[63] H. Pitsch, M. Chen, N. Peters, Unsteady flamelet modeling of turbulent hydrogen-air diffusion flames, Symposium (International) on Combustion 27 (1) (1998) 1057 – 1064.

[64] M. Ihme, H. Pitsch, Modeling of radiation and nitric oxide formation in turbulent nonpremixed flames using a flamelet/progress variable formulation, Physics of Fluids 20 (5) (2008) 055110.

[65] M. Ravikanti, M. Hossain, W. Malalasekera, Laminar flamelet model prediction of NOx formation in a turbulent bluff-body combustor, Proceedings of the Institution of Mechanical Engineers, Part A: Journal of Power and Energy 223 (1) (2009) 41–54.

[66] T. Shimizu, F. A. Williams, A. Frassoldati, Concentrations of nitric oxide in laminar counterflow methane/air diffusion flames, Journal of propulsion and power 21 (6) (2005) 1019–1028.

[67] R. Ravikrishna, N. M. Laurendeau, Laser-induced fluorescence measurements and modeling of nitric oxide in methane–air and ethane–air counterflow diffusion flames, Combustion and flame 120 (3)

(2000) 372–382.

[68] G. Rørtveit, J. Hustad, NO_x Formations in Diluted CH_4/H_2 Counterflow Diffusion Flames, International Journal of Energy for a Clean Environment 4 (4) (2003) 303–314.

[69] M. Mueller, G. Blanquart, H. Pitsch, Hybrid method of moments for modeling soot formation and growth, Combustion and Flame 156 (6) (2009) 1143–1155.

[70] C. Saggese, S. Ferrario, J. Camacho, A. Cuoci, A. Frassoldati, E. Ranzi, H. Wang, T. Faravelli, Kinetic modeling of particle size distribution of soot in a premixed burner-stabilized stagnation ethylene flame, Combustion and Flame 162 (9) (2015) 3356–3369.

[71] A. Violi, A. F. Sarofim, G. A. Voth, Kinetic Monte Carlo–molecular dynamics approach to model soot inception, Combustion science and technology 176 (5-6) (2004) 991–1005.

[72] S.-C. Kong, Y. Sun, R. D. Rietz, Modeling diesel spray flame liftoff, sooting tendency, and NOx emissions using detailed chemistry with phenomenological soot model, Journal of Engineering for Gas Turbines and Power 129 (1) (2007) 245–251.